

# Passive control of multiple structural resonances with piezoelectric vibration absorbers

G. Raze<sup>a,\*</sup>, J. Dietrich<sup>a</sup>, G. Kerschen<sup>a</sup>

<sup>a</sup>*Space Structures and Systems Laboratory, Aerospace and Mechanical Engineering Department, University of Liège  
Quartier Polytech 1 (B52/3), Allée de la Découverte 9, B-4000 Liège, Belgium*

---

## Abstract

A novel sequential tuning procedure for passive piezoelectric shunts targeting multiple structural modes is proposed in this work. The control authority on each targeted mode can be quantitatively chosen ab initio and is shown to be limited by passivity requirements, which highlights the fundamental limitations of multimodal piezoelectric shunts. Based on effective characteristics of the piezoelectric system around resonance, electrical damping ratios and resonance frequencies are derived using well-established single-mode formulae from the literature, thereby fully specifying the characteristics of the shunt impedance. The proposed approach is numerically verified and experimentally validated on piezoelectric beams by emulating the shunt with a digital vibration absorber.

*Keywords:* Passive control law, Multimodal vibration mitigation, Piezoelectric shunt, Digital control

---

## 1. Introduction

Piezoelectric shunt damping is a passive vibration control technique aiming to mitigate the vibrations of a host structure [1]. A piezoelectric transducer bonded to this structure converts part of its mechanical energy to electrical energy, which can then be dissipated into an electrical circuit shunting the electrodes of the transducer. Shunts can be of resistive or resonant type, and are traditionally optimized to reduce the vibrations around one specific mode [2–5]. Reviews on the subject can be found in [6–8].

Several approaches were proposed to extend resonant piezoelectric shunt damping to the control of multiple modes. Among them, one consists in designing more complex shunts that resonate with the inherent capacitance of the piezoelectric transducer at multiple frequencies. Several ad hoc circuit topologies were proposed to fulfill this objective [9–13]. Some of these works proposed associated tuning formulae for the electrical parameters, but these problems were shown to be rather complex due to the interaction between the different resonant branches, and numerical optimization was often called upon to tune these parameters [14–18]. Although numerical optimization is a powerful tool and could even be used for real-time tuning of shunts [19], it is a time-consuming process whose outcome may be a local optimum. To address this, a sequential tuning procedure based on

---

\*Corresponding author

*Email addresses:* [g.raze@uliege.be](mailto:g.raze@uliege.be) (G. Raze), [jdietrich@uliege.be](mailto:jdietrich@uliege.be) (J. Dietrich), [g.kerschen@uliege.be](mailto:g.kerschen@uliege.be) (G. Kerschen)

effective characteristics associated with electrical resonances was proposed in [20]. However, this procedure is specifically designed for a particular shunt topology, does not provide a quantitative insight into the arbitrary choices made beforehand, and relies on an ad hoc identification procedure which may fail for structures with, e.g., closely-spaced modes.

Focusing now on the realization of the control system, resonant piezoelectric shunts are seldom implemented with passive elements, mainly because the required inductances are typically large. Although it is possible to manufacture them [21], this problem remains challenging and a common workaround consists in using synthetic inductors [22]. Alternatively, a digital vibration absorber (DVA) can be used [23]. By combining a current source with a digital unit, virtually any circuit can be emulated, which provides this approach with an exceptional versatility.

This work proposes a novel sequential specification procedure to tune passive and generic piezoelectric shunts targeting multiple electrical resonances. Limitations on performance due to passivity are highlighted, as well as trade-offs that must be made on the control authority on the targeted modes. The resulting shunt is realized experimentally using a DVA. This article is organized as follows. Section 2 first introduces models of piezoelectric structures and shunts targeting a single resonant mode. Section 3 then presents a sequential specification procedure for shunts targeting multiple modes. The realization of such shunts with a DVA is discussed in Section 4. Eventually, the theoretical developments are numerically verified and experimentally validated in Sections 5 and 6, respectively. Conclusions on the present work are drawn in Section 7.

## 2. Modeling piezoelectric structures with a single piezoelectric transducer

Models of piezoelectric structures can be obtained, e.g., analytically [13], via a Rayleigh-Ritz approach [24] or the finite element method [25]. The electrical variables associated with the continuous electrodes of the transducers are discretized by considering only their voltage and charge. Structures with a single piezoelectric transducer are considered herein. Alternatively, one can also consider structures with multiple transducers where the electrodes are connected either in series or in parallel, resulting in an equivalent transducer with a single electrical port. Introducing the vector of  $N$  generalized mechanical degrees of freedom (DoFs)  $\mathbf{x}$ , the vector of generalized mechanical loading  $\mathbf{f}$  of length  $N$ , the voltage across the electrodes of the transducer  $V$  and the charge flowing through it  $q$ , the governing equations of the piezoelectric structure read

$$\begin{cases} \mathbf{M}\ddot{\mathbf{x}} + \mathbf{K}_{\text{sc}}\mathbf{x} + \boldsymbol{\gamma}_p V = \mathbf{f} \\ \boldsymbol{\gamma}_p^T \mathbf{x} - C_p^\varepsilon V = q \end{cases} \quad (1)$$

In these equations,  $\mathbf{M}$  is the  $N \times N$  structural mass matrix,  $\mathbf{K}_{\text{sc}}$  is the  $N \times N$  structural stiffness matrix when the transducer is short-circuited,  $\boldsymbol{\gamma}_p$  is a piezoelectric coupling vector of length  $N$  and  $C_p^\varepsilon$  is the piezoelectric capacitance at constant strain. Alternatively, the piezoelectric voltage may be used as independent variable. After inversion of the electrical equation, the governing equations become

$$\begin{cases} \mathbf{M}\ddot{\mathbf{x}} + \mathbf{K}_{\text{oc}}\mathbf{x} - \boldsymbol{\theta}_p q = \mathbf{f} \\ \boldsymbol{\theta}_p^T \mathbf{x} - \frac{1}{C_p^\varepsilon} q = V \end{cases} \quad (2)$$

where

$$\mathbf{K}_{\text{oc}} = \mathbf{K}_{\text{sc}} + \frac{1}{C_p^\varepsilon} \boldsymbol{\gamma}_p \boldsymbol{\gamma}_p^T, \quad \boldsymbol{\theta}_p = \frac{1}{C_p^\varepsilon} \boldsymbol{\gamma}_p \quad (3)$$

are the open-circuit stiffness matrix and a piezoelectric coupling vector, respectively.

### 2.1. Short-circuit and open-circuit modes

The short-circuit modes are the resonant modes of the structure when the transducer is short-circuited ( $V = 0$ ). They satisfy the following generalized eigenvalue problem

$$\mathbf{K}_{\text{sc}} \Phi_{\text{sc}} = \mathbf{M} \Phi_{\text{sc}} \Omega_{\text{sc}}^2, \quad \Omega_{\text{sc}} = \begin{bmatrix} \omega_{\text{sc},1} & & \\ & \ddots & \\ & & \omega_{\text{sc},N} \end{bmatrix} \quad (4)$$

where  $\Phi_{\text{sc}}$  is the matrix of short-circuit mode shapes and  $\Omega_{\text{sc}}$  is a diagonal matrix containing the short-circuit resonance frequencies  $\omega_{\text{sc},n}$ . The mode shapes are usually mass-normalized, i.e.,

$$\Phi_{\text{sc}}^T \mathbf{M} \Phi_{\text{sc}} = \mathbf{I}, \quad \Phi_{\text{sc}}^T \mathbf{K}_{\text{sc}} \Phi_{\text{sc}} = \Omega_{\text{sc}}^2, \quad (5)$$

where  $\mathbf{I}$  is the identity matrix. If the generalized DoFs are expressed in terms of short-circuit modal amplitudes  $\boldsymbol{\eta}_{\text{sc}}$  as

$$\mathbf{x}(t) = \Phi_{\text{sc}} \boldsymbol{\eta}_{\text{sc}}(t), \quad (6)$$

then, Eq. (1) can be rewritten, after premultiplication of the mechanical equation by  $\Phi_{\text{sc}}^T$ , as

$$\begin{cases} \ddot{\boldsymbol{\eta}}_{\text{sc}} + \Omega_{\text{sc}}^2 \boldsymbol{\eta}_{\text{sc}} + \Phi_{\text{sc}}^T \boldsymbol{\gamma}_p V = \Phi_{\text{sc}}^T \mathbf{f} \\ \boldsymbol{\gamma}_p^T \Phi_{\text{sc}} \boldsymbol{\eta}_{\text{sc}} - C_p^\epsilon V = q \end{cases} \quad (7)$$

Similar developments can be made with the open-circuit modes, which are the resonant modes of the structures with the transducer open-circuited ( $q = 0$ ). They satisfy the following generalized eigenvalue problem

$$\mathbf{K}_{\text{oc}} \Phi_{\text{oc}} = \mathbf{M} \Phi_{\text{oc}} \Omega_{\text{oc}}^2, \quad \Omega_{\text{oc}} = \begin{bmatrix} \omega_{\text{oc},1} & & \\ & \ddots & \\ & & \omega_{\text{oc},N} \end{bmatrix} \quad (8)$$

where  $\Phi_{\text{oc}}$  is the matrix of mass-normalized open-circuit mode shapes and  $\Omega_{\text{oc}}$  is a diagonal matrix containing the open-circuit resonance frequencies  $\omega_{\text{oc},n}$ . Using open-circuit modal amplitudes  $\boldsymbol{\eta}_{\text{oc}}$ , Eq. (2) can also be rewritten as

$$\begin{cases} \ddot{\boldsymbol{\eta}}_{\text{oc}} + \Omega_{\text{oc}}^2 \boldsymbol{\eta}_{\text{oc}} - \Phi_{\text{oc}}^T \boldsymbol{\theta}_p q = \Phi_{\text{oc}}^T \mathbf{f} \\ \boldsymbol{\theta}_p^T \Phi_{\text{oc}} \boldsymbol{\eta}_{\text{oc}} - \frac{1}{C_p^\epsilon} q = V \end{cases} \quad (9)$$

### 2.2. Dynamic capacitance

Assuming that the structure is unforced ( $\mathbf{f} = \mathbf{0}$ ), taking the Laplace transform of the mechanical equation in Eq. (7) and inserting it into the electrical equation gives a dynamic relation between  $V$  and  $q$ , the *dynamic capacitance*  $C_p(s)$  [26]:

$$- \left[ C_p^\epsilon + \boldsymbol{\gamma}_p^T \Phi_{\text{sc}} (s^2 \mathbf{I} + \Omega_{\text{sc}}^2)^{-1} \Phi_{\text{sc}}^T \boldsymbol{\gamma}_p \right] V = -C_p^\epsilon \left[ 1 + \sum_{n=1}^N \frac{\gamma_{\phi,n}^2}{C_p^\epsilon} \frac{1}{s^2 + \omega_{\text{sc},n}^2} \right] V = C_p(s) V = q, \quad (10)$$

where  $s$  is Laplace's variable and the modal coupling coefficients  $\gamma_{\phi,n}$  are given by

$$\boldsymbol{\gamma}_p^T \Phi_{\text{sc}} = [\gamma_{\phi,1} \quad \cdots \quad \gamma_{\phi,N}]. \quad (11)$$

Applying an identical procedure starting from the open-circuit configuration (Eq. (9)) yields the inverse transfer function, the *dynamic elastance*  $E_p(s)$ , as

$$-\left[\frac{1}{C_p^\varepsilon} - \boldsymbol{\theta}_p^T \boldsymbol{\Phi}_{\text{oc}} (s^2 \mathbf{I} + \boldsymbol{\Omega}_{\text{oc}}^2)^{-1} \boldsymbol{\Phi}_{\text{oc}}^T \boldsymbol{\theta}_p\right] q = -\frac{1}{C_p^\varepsilon} \left[1 - \sum_{n=1}^N \frac{C_p^\varepsilon \theta_{\phi,n}^2}{s^2 + \omega_{\text{oc},n}^2}\right] q = E_p(s)q = V, \quad (12)$$

where the modal coupling coefficients  $\theta_{\phi,n}$  are given by

$$\boldsymbol{\theta}_p^T \boldsymbol{\Phi}_{\text{oc}} = [\theta_{\phi,1} \quad \cdots \quad \theta_{\phi,N}]. \quad (13)$$

Eqs. (10) and (12) show that the poles of the dynamic capacitance (elastance) are the short-circuit (open-circuit) resonance frequencies. Furthermore, since the dynamic capacitance (elastance) is the inverse of the dynamic elastance (capacitance), the zeros of the former are the poles of the latter, i.e., the open-circuit (short-circuit) resonance frequencies. Therefore, an alternate expression for the dynamic capacitance is

$$C_p(s) = -C_p^\varepsilon \frac{\prod_{n=1}^N (s^2 + \omega_{\text{oc},n}^2)}{\prod_{n=1}^N (s^2 + \omega_{\text{sc},n}^2)} = \frac{1}{E_p(s)}. \quad (14)$$

Eq. (10) indicates that the coefficients  $\gamma_{\phi,n}^2/C_p^\varepsilon$  can be thought of as residues associated with the poles  $\pm j\omega_{\text{sc},n}$ . The cover-up method [27] can be used to deduce them from the short- and open-circuit resonance frequencies and the piezoelectric capacitance  $C_p^\varepsilon$  with Eq. (14). Indeed, equating Eqs. (10) and (14), multiplying them by  $s^2 + \omega_{\text{sc},r}^2$  and equating their limit for  $s \rightarrow j\omega_{\text{sc},r}$  yields

$$\gamma_{\phi,r}^2 = C_p^\varepsilon \frac{\prod_{n=1}^N (\omega_{\text{oc},n}^2 - \omega_{\text{sc},r}^2)}{\prod_{n=1, n \neq r}^N (\omega_{\text{sc},n}^2 - \omega_{\text{sc},r}^2)}. \quad (15)$$

Similar developments from Eq. (12) yield

$$\theta_{\phi,r}^2 = -\frac{1}{C_p^\varepsilon} \frac{\prod_{n=1}^N (\omega_{\text{sc},n}^2 - \omega_{\text{oc},r}^2)}{\prod_{n=1, n \neq r}^N (\omega_{\text{oc},n}^2 - \omega_{\text{oc},r}^2)}. \quad (16)$$

Eqs. (15) and (16) give a practical way to evaluate the modal coupling coefficients experimentally from simple measurements of the resonance frequencies and the piezoelectric capacitance  $C_p^\varepsilon$ . As shall be shown in the sequel, this is sufficient to tune a shunt with multiple resonance frequencies.

### 2.3. Electromechanical coupling factors

The electromechanical coupling between mode  $n$  and a piezoelectric transducer can be assessed quantitatively with a dimensionless quantity called the modal electromechanical coupling factor (MEMCF) [25]

$$K_{c,n}^2 = \frac{\omega_{oc,n}^2 - \omega_{sc,n}^2}{\omega_{sc,n}^2}. \quad (17)$$

This quantity can be used to predict the vibration reduction brought by resonant shunts (see, e.g., [28]). In general, the greater the MEMCF, the greater the attenuation.

### 2.4. Structures with piezoelectric shunts

Single-mode resonant shunts can be used to mitigate a specific mode, and their tuning will be used as a baseline in Section 3.

#### 2.4.1. Series RL shunt

Upon connecting the electrodes of a transducer to a series RL shunt, the voltage and charge become related by

$$V = (Ls^2 + Rs)q = sZ_s(s)q, \quad (18)$$

where  $L$ ,  $R$  and  $Z_s$  are the shunt inductance, resistance and impedance, respectively. Closed-form solutions leading to optimal amplitude reduction have been found in [4, 5] in the case of a single-degree-of-freedom (SDoF) structure. Using these formulae (see Appendix A) for a shunt targeting mode  $n$  and neglecting every other structural mode, the optimal inductance and resistance are

$$L = \frac{1}{\delta^2(K_{c,n})\omega_{oc,n}^2 C_p^\epsilon}, \quad R = \frac{2\zeta(K_{c,n})}{\delta(K_{c,n})\omega_{oc,n} C_p^\epsilon}, \quad (19)$$

respectively, where  $\delta$  and  $\zeta$  are electrical frequency and damping ratios for the series RL case, respectively. It is possible to enhance these tuning rules for multiple-degree-of-freedom structures by accounting for the influence of non-resonant modes [29, 30], and this approach shall be adopted hereafter when tuning circuits with multiple electrical resonances.

#### 2.4.2. Parallel RL shunt

Alternatively to the series RL case, a parallel RL shunt can be employed, leading to the following relation between charge and voltage

$$q = \left( \frac{B}{s^2} + \frac{G}{s} \right) V = \frac{Y_s(s)}{s} V, \quad (20)$$

where  $B$ ,  $G$  and  $Y_s$  are the shunt reluctance, conductance and admittance, respectively. The exact  $H_\infty$ -optimal solution for a SDof structure was derived by Ikegame et al [5]. The optimal single-mode reluctance  $B$  and conductance  $G$  for a shunt targeting mode  $n$  are given by

$$B = \nu^2 (K_{c,n}) \omega_{sc,n}^2 C_p^\epsilon, \quad G = 2\zeta (K_{c,n}) \nu (K_{c,n}) \omega_{sc,n} C_p^\epsilon, \quad (21)$$

respectively (see Appendix A).  $\nu$  and  $\zeta$  are electrical frequency and damping ratios for the parallel RL case, respectively.

### 3. Specification method for multimodal control

It is now sought to generalize the piezoelectric shunt presented in Section 2.4 to the control of multiple modes with a direct tuning method. A lossless shunt with the most general form of immittance is first considered. It will then be demonstrated that the immittance of an equivalent circuit resulting from the connection of the piezoelectric transducer with this lossless circuit takes a specific form. This immittance can be expanded in partial fractions, where the resonance frequencies of the circuit are directly identifiable. Associated with these frequencies are residues (that can be seen as resonance amplitudes squared) which characterize the electromechanical coupling existing between the mechanical and electrical resonances.

With this partial fraction expansion and a few simplifying assumptions, it is possible to show that the problem can be put into a simpler form similar to the SDoF case. Specifically, *effective* short- and open-circuit resonance frequencies can be evaluated to compute an effective MEMCF. These effective frequencies may differ from those of the structure because the circuit itself influences them. From there on, a specification procedure can be devised. The procedure takes as input the resonance frequencies of the piezoelectric structure, the piezoelectric capacitance at constant strain, a set of modes to be controlled and a set of associated residues, which characterize the control authority on these modes. For each targeted mode, the tuning formulae presented in Section 2.4 are used with the effective characteristics to sequentially specify the characteristics of the immittance in terms of zeros frequencies and damping ratios. The determination of the shunt admittance and its realization are discussed in the next section.

#### 3.1. Admittance-based model

##### 3.1.1. Norton's equivalent admittance

The connection of a shunt of admittance  $Y_s$  to the electrodes of the piezoelectric transducer imposes the following voltage-to-charge relation

$$q = \frac{Y_s(s)}{s} V. \quad (22)$$

Inserting this relation into Eq. (7), the governing equations for the coupled system are obtained as

$$\begin{cases} (s^2 \mathbf{I} + \mathbf{\Omega}_{sc}^2) \boldsymbol{\eta}_{sc} + \boldsymbol{\Phi}_{sc}^T \boldsymbol{\gamma}_p V = \boldsymbol{\Phi}_{sc}^T \mathbf{f} \\ \frac{Y_N(s)}{s} V - \boldsymbol{\gamma}_p^T \boldsymbol{\Phi}_{sc} \boldsymbol{\eta}_{sc} = 0 \end{cases} \quad (23)$$

in which

$$Y_N(s) = sC_p^\varepsilon + Y_s(s) \quad (24)$$

is Norton's equivalent admittance of the parallel connection of the shunt with a capacitor of capacitance  $C_p^\varepsilon$ , as schematized in Fig. 1.

The problem described by Eq. 23 is equivalent to the feedback control one depicted in Fig. 1(c), where  $sY_N^{-1}(s)$  plays the same role as a controller. Upon connecting an inductor of reluctance  $B$  (i.e., a lossless RL shunt) to the transducer, the transfer function of this equivalent controller takes the form

$$\frac{s}{Y_N(s)} = \frac{s}{sC_p^\varepsilon + \frac{B}{s}} = \frac{1}{C_p^\varepsilon} \frac{s^2}{s^2 + \omega_e^2}, \quad (25)$$

whose resonance frequency is the electrical one given by  $\omega_e^2 = B/C_p^\varepsilon$ .

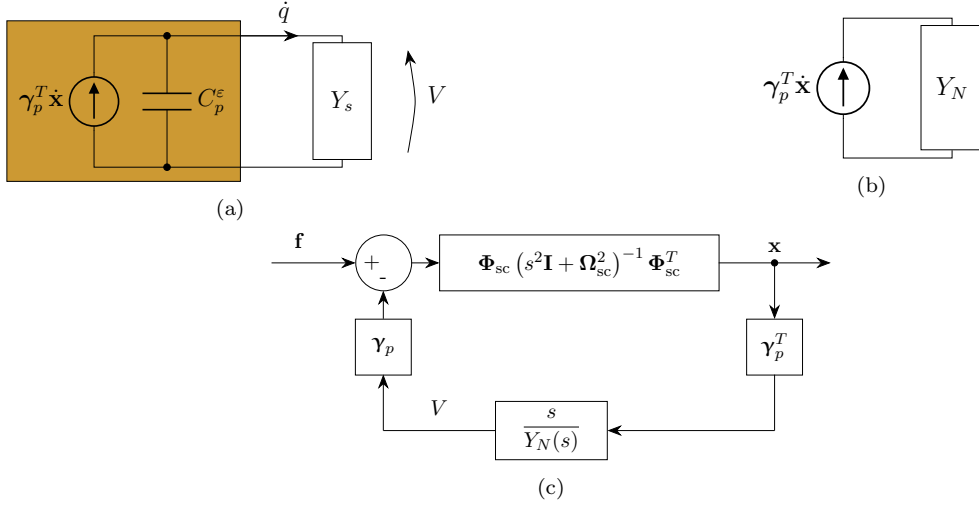


Figure 1: Shunt connected to a piezoelectric transducer (a), Norton's equivalent model (b) and equivalent feedback control problem (c).

### 3.1.2. Implications of Foster's reactance theorem

Considering now a more general shunt made up of passive reactive lossless elements, Foster's reactance theorem [31, 32] stipulates that its admittance must be of the form

$$Y_s(s) = K_s \frac{s \prod_{i=1}^{N_z} (s^2 + z_{s,i}^2)}{\prod_{i=1}^{N_p} (s^2 + p_{s,i}^2)} \quad (26)$$

with  $K_s > 0$ ,

$$0 \leq p_{s,1} < z_{s,1} < p_{s,2} < z_{s,2} < \dots \quad (27)$$

and either  $N_z = N_p - 1$  or  $N_z = N_p$ . Inserting Eq. (26) into Eq. (24) gives

$$\frac{s}{Y_N(s)} = \frac{s}{sC_p^\epsilon + Y_s(s)} = \frac{\prod_{i=1}^{N_p} (s^2 + p_{s,i}^2)}{C_p^\epsilon \prod_{i=1}^{N_p} (s^2 + p_{s,i}^2) + K_s \prod_{i=1}^{N_z} (s^2 + z_{s,i}^2)}. \quad (28)$$

The degree of the numerator and that of the denominator are equal given that  $N_z \leq N_p$ , and thus this transfer function is always biproper. Moreover, it cannot possess a pole at  $s = 0$  but may have a double zero at  $s = 0$  (if  $p_{s,1} = 0$ ). Therefore, it takes the general form

$$\frac{s}{Y_N(s)} = \frac{1}{C_p^\epsilon} \left( r_0 + \sum_{i=1}^{N_s} \frac{r_i s^2}{s^2 + z_i^2} \right), \quad (29)$$

where  $z_i$  is a zero of Norton's admittance, and  $r_i$  is its associated residue. It can be noted that the terms in the sum featured in Eq. (29), which correspond to electrical resonances, have the same form as Eq. (25).

### 3.1.3. Passivity constraints

Foster's reactance theorem [31] can also be used to set limitations on the values that the residues can take. First of all, because the parallel connection of a passive circuit with a capacitor makes up a circuit which is itself passive, every residue  $r_i$  must be positive. Second, by equating Eqs. (28) and (29) for  $s \rightarrow \infty$ , it is remarked that

$$\lim_{s \rightarrow \infty} \frac{s}{Y_N(s)} = \lim_{s \rightarrow \infty} \frac{\prod_{i=1}^{N_p} (s^2 + p_{s,i}^2)}{C_p^\varepsilon \prod_{i=1}^{N_p} (s^2 + p_{s,i}^2) + K_s \prod_{i=1}^{N_z} (s^2 + z_{s,i}^2)} = \frac{1}{C_p^\varepsilon} \sum_{i=0}^{N_s} r_i. \quad (30)$$

Hence, if  $N_z = N_p - 1$ ,

$$\frac{1}{C_p^\varepsilon} \sum_{i=0}^{N_s} r_i = \frac{1}{C_p^\varepsilon}, \quad (31)$$

and if  $N_z = N_p$ ,

$$\frac{1}{C_p^\varepsilon} \sum_{i=0}^{N_s} r_i = \frac{1}{C_p^\varepsilon + K_s} \in \left[ 0, \frac{1}{C_p^\varepsilon} \right]. \quad (32)$$

The foregoing developments show that the residues must satisfy the passivity constraints

$$r_i \geq 0 \quad \forall i \in [0, N_s], \quad 0 \leq \sum_{i=0}^{N_s} r_i \leq 1. \quad (33)$$

It shall be shown that the last constraint places fundamental limits on the performance of multi-modal shunts.

### 3.1.4. Background contributions

In the remainder of this section, it is assumed that mode  $k$  of Norton's admittance targets resonance  $r$  of the structure. Non-resonant mechanical modes are identified by a subscript  $n$  ( $n = 1, \dots, r-1, r+1, \dots, N$ ). The external forcing is also assumed to be zero in order to characterize the poles of the system. Since the structural matrices are diagonal, the non-resonant modal coordinates may be expressed using Eq. (23) as a sole function of  $V$

$$\eta_{sc,n} = -\frac{\gamma_{\phi,n}}{s^2 + \omega_{sc,n}^2} V, \quad (34)$$

which, inserted back into the electrical equation, yields

$$\begin{cases} (s^2 + \omega_{sc,r}^2) \eta_{sc,r} + \gamma_{\phi,r} V = 0 \\ \left( \frac{Y_N(s)}{s} + \sum_{n=1, n \neq r}^N \frac{\gamma_{\phi,n}^2}{s^2 + \omega_{sc,n}^2} \right) V - \gamma_{\phi,r} \eta_{sc,r} = 0 \end{cases}. \quad (35)$$

Finally, expressing  $V$  as a function of  $\eta_{sc,r}$  and substituting the resulting expression into the mechanical equation, one gets

$$\left( s^2 + \omega_{sc,r}^2 + \frac{\gamma_{\phi,r}^2}{C_p^\varepsilon} \frac{C_p^\varepsilon \frac{s}{Y_N(s)}}{1 + C_p^\varepsilon \frac{s}{Y_N(s)} \sum_{n=1, n \neq r}^N \frac{\gamma_{\phi,n}^2}{C_p^\varepsilon} \frac{1}{s^2 + \omega_{sc,n}^2}} \right) \eta_{sc,r} = 0. \quad (36)$$

So far, no approximation was made. However, Eq. (36) is potentially of high order in  $s$  and thus complicated to work with. Moreover, it also requires the knowledge of every characteristic from Norton's admittance ( $r_i$  and  $z_i$  for each electrical mode), which would not ease its use within a specification procedure. Approximations shall thus be made to simplify the problem. The first approximation is a classical one and regards the non-resonant mechanical modes [29]. From their contribution given in Eq. (36), only the static contribution from modes with frequency higher than  $\omega_{sc,r}$  is retained (the other contribution decaying in  $s^{-2}$ ). In other words,

$$\sum_{n=1, n \neq r}^N \frac{\gamma_{\phi,n}^2}{C_p^\varepsilon} \frac{1}{s^2 + \omega_{sc,n}^2} \approx \sum_{n=r+1}^N \frac{\gamma_{\phi,n}^2}{\omega_{sc,n}^2 C_p^\varepsilon}. \quad (37)$$

The second approximation consists in similarly simplifying the dynamics of non-resonant electrical modes. Electrical modes whose frequency is lower and higher than  $z_k$  are assumed to be capacitively- and inductively-dominated, i.e.,

$$\frac{r_i s^2}{s^2 + z_i^2} \approx r_i, \quad i < k, \quad \text{and} \quad \frac{r_i s^2}{s^2 + z_i^2} \approx \frac{r_i s^2}{z_i^2}, \quad i > k, \quad (38)$$

respectively.

For conciseness, the following dimensionless quantities are introduced

$$\kappa_{\bar{r}} = \sum_{n=r+1}^N \frac{\gamma_{\phi,n}^2}{\omega_{sc,n}^2 C_p^\varepsilon}, \quad \kappa_r = \sum_{n=r}^N \frac{\gamma_{\phi,n}^2}{\omega_{sc,n}^2 C_p^\varepsilon}, \quad (39)$$

representing the static influence from higher-frequency modes without and with mode  $r$ , respectively, and

$$y_l = \sum_{i=0}^{k-1} r_i, \quad y_h = \sum_{i=k+1}^{N_s} \frac{r_i \omega_{sc,r}^2}{z_i^2}, \quad (40)$$

representing the influence of capacitively-dominated and inductively-dominated electrical modes, respectively. It can be remarked that computing  $y_l$  and  $y_h$  requires the knowledge of all the residues but only the zeros from higher-frequency modes. Using the simplifying assumptions (Equations (37)-(38)) into Eq. (36), a dynamic equation of lower order including the background contribution of non-resonant mechanical and electrical modes is obtained as

$$\left( s^2 + \omega_{sc,r}^2 + \omega_{sc,r}^2 (\kappa_r - \kappa_{\bar{r}}) \frac{y_l + \frac{r_k s^2}{s^2 + z_k^2} + y_h \frac{s^2}{\omega_{sc,r}^2}}{1 + \kappa_{\bar{r}} \left( y_l + \frac{r_k s^2}{s^2 + z_k^2} + y_h \frac{s^2}{\omega_{sc,r}^2} \right)} \right) \eta_{sc,r} = 0. \quad (41)$$

### 3.1.5. Effective short-circuit and open-circuit resonance frequencies

Going back to the single-mode case, Section 2.4 highlighted the relevance of short- and open-circuit resonance frequencies for tuning. In these cases, associated Norton's equivalent admittances are, using Eq. (24),

$$\frac{s}{Y_{N,sc}} = \frac{s}{Y_N} \Big|_{Y_s=\infty} = 0, \quad \frac{s}{Y_{N,oc}} = \frac{s}{Y_N} \Big|_{Y_s=0} = \frac{1}{C_p^\epsilon}. \quad (42)$$

By analogy, we define modal short circuit and modal open circuit Norton's admittances by replacing the resonant term by its asymptotic values for  $s \rightarrow 0$  and  $s \rightarrow \infty$ , respectively. In other words, the resonant electrical term can be replaced by

$$\lim_{s \rightarrow 0} \frac{r_k s^2}{s^2 + z_k^2} = 0 \quad \text{and} \quad \lim_{s \rightarrow \infty} \frac{r_k s^2}{s^2 + z_k^2} = r_k, \quad (43)$$

in the case of a modal short circuit and modal open circuit, respectively. Substituting these expressions into Eq. (41) defines effective resonance frequencies. Based on their value, it is possible to assess an MEMCF which will eventually be used to specify the characteristics of the shunt.

Substituting the electrical resonant term by zero in Eq. (41) gives a quadratic equation in  $s^2$ . The effective short-circuit resonance frequency  $\widehat{\omega}_{sc,r}$  can be found by solving this equation for  $s = j\widehat{\omega}_{sc,r}$  as

$$\widehat{\omega}_{sc,r} = \frac{\omega_{sc,r}}{\sqrt{\frac{1 + y_l \kappa_{\bar{r}} + y_h \kappa_r}{2 + 2y_l \kappa_r} + \sqrt{\left(\frac{1 + y_l \kappa_{\bar{r}} + y_h \kappa_r}{2 + 2y_l \kappa_r}\right)^2 - \frac{y_h \kappa_{\bar{r}}}{1 + y_l \kappa_r}}}}. \quad (44)$$

Substituting the resonant term by  $r_k$ , the effective open-circuit resonance frequency  $\widehat{\omega}_{oc,r}$  can be estimated by

$$\widehat{\omega}_{oc,r} = \frac{\omega_{sc,r}}{\sqrt{\frac{1 + (y_l + r_k) \kappa_{\bar{r}} + y_h \kappa_r}{2 + 2(y_l + r_k) \kappa_r} + \sqrt{\left(\frac{1 + (y_l + r_k) \kappa_{\bar{r}} + y_h \kappa_r}{2 + 2(y_l + r_k) \kappa_r}\right)^2 - \frac{y_h \kappa_{\bar{r}}}{1 + (y_l + r_k) \kappa_r}}}}. \quad (45)$$

### 3.1.6. Coupling assessment

Eq. (17) can be replaced by an MEMCF based on the effective short- and open-circuit resonance frequencies

$$\widehat{K}_{c,r}^2 = \frac{\widehat{\omega}_{oc,r}^2 - \widehat{\omega}_{sc,r}^2}{\widehat{\omega}_{sc,r}^2}. \quad (46)$$

We note the following particular cases

$$\widehat{K}_{c,r}^2 \Big|_{r_k=0} = 0, \quad \widehat{K}_{c,r}^2 \Big|_{r_k=1} = K_{c,r}^2 \quad (47)$$

and it is possible to show that  $\widehat{\omega}_{oc,r}$  is a growing function of  $r_k$ , and thus so is  $\widehat{K}_{c,r}$ .

A more explicit expression of  $\widehat{K}_{c,r}$  as a function of  $r_k$  can be obtained if one neglects the influence of non-resonant terms ( $y_l = y_h = \kappa_{\bar{r}} = 0$ ). The MEMCF is then approximated by

$$\widehat{K}_{c,r}^2 \approx r_k \frac{\gamma_{\phi,r}^2}{\omega_{sc,r}^2 C_p^\epsilon} \approx r_k K_{c,r}^2, \quad (48)$$

where  $K_{c,r}^2$  is approximated under the same assumptions (i.e., starting from Eq. (7) and neglecting the contribution from non-resonant mechanical modes [25]). Eq. (48) gives a remarkably concise expression of the MEMCF as a function of the residue. It can be used as an approximate quantitative guide to select a set of residues based on the performance desired for specific modes. In any case, the greater the residue associated to one mode, the greater the MEMCF. From Eq. (33), it is noted that a residue cannot be greater than unity, and in case it is unitary all the other residues are zero. Thus, regarding a specific mode, a passive multimodal shunt can at best perform as well as a single-mode shunt. When multiple modes are targeted, performance on one mode has to be traded for performance on the other modes. This highlights a fundamental limitation in performance that can be expected from passive multimodal shunts.

It can also be noted that the residue  $r_0$  in Eq. (29) is not associated to any mode, but still intervenes in the passivity constraint (Eq. (33)). Hence, in terms of vibration reduction,  $r_0 = 0$  is desirable to maximize the value of the other residues.

### 3.1.7. Specifications for the shunt

The previous developments can be assembled into a tuning procedure, which goes as follows. The user first selects the modes to be controlled and their associated residues, knowing that the latter will quantify the electromechanical coupling with the former, and ultimately the amplitude reduction. Typically, Eq. (48) can be used at this stage to predict the MEMCF. The tuning procedure then consists in defining the zeros of Norton's equivalent admittance  $z_k$  and to add dissipation to the circuit through specification of associated damping ratios  $\zeta_k$  in order to provide nearly-optimal vibration reduction.

From the tuning formulae of the SDoF case, the electrical resonance frequency can be computed from the MEMCF and the effective resonance frequencies as

$$\omega_{e,k} = \delta \left( \widehat{K}_{c,r} \right) \widehat{\omega}_{oc,r} \quad \text{or} \quad \omega_{e,k} = \nu \left( \widehat{K}_{c,r} \right) \widehat{\omega}_{sc,r}, \quad (49)$$

depending on whether the circuit has to be tuned based on the series RL (Eq. (A.2)) or parallel RL (Eq. (A.6)) SDoF baseline case, respectively<sup>1</sup>. From Eq. (41), the electrical resonance frequency  $\omega_{e,k}$  of the lossless circuit creates a zero in the mechanical receptance if

$$1 + \kappa_{\bar{r}} \left( y_l + \frac{r_k s^2}{s^2 + z_k^2} + y_h \frac{s^2}{\omega_{sc,r}^2} \right) = 0 \quad (50)$$

for  $s = j\omega_{e,k}$ . Solving for  $z_k$  eventually yields

$$z_k = \omega_{e,k} \sqrt{1 + \frac{r_k}{\frac{1}{\kappa_{\bar{r}}} + y_l - y_h \frac{\omega_{e,k}^2}{\omega_{sc,r}^2}}}. \quad (51)$$

In order to avoid the appearance of new undamped resonances in the mechanical compliance, dissipative elements can be added to the shunt, similarly to the SDoF case [2, 3]. Herein, their effect is modeled by electrical modal damping ratios. They can be determined as

$$\zeta_k = \zeta \left( \widehat{K}_{c,r} \right) \quad \text{or} \quad \zeta_k = \varsigma \left( \widehat{K}_{c,r} \right), \quad (52)$$

<sup>1</sup>Other tuning formulae for the series or parallel RL shunts [2, 3, 28, 33, 34] can also be used.

depending on the baseline case: series RL (Eq. (A.3)) or parallel RL (Eq. (A.7)) SDoF, respectively. In general, the best-suited baseline case will depend on the topology of the dissipative shunt.

From Eq. (38), it is seen that when tuning  $z_k$ ,  $z_{k+1}$  to  $z_{N_s}$  have to be known. In order to have a sequential specification procedure where everything is known when considering resonance  $k$ , this suggests that the electrical resonances have to be specified in descending order of frequency. Fig. 2 summarizes the proposed approach.

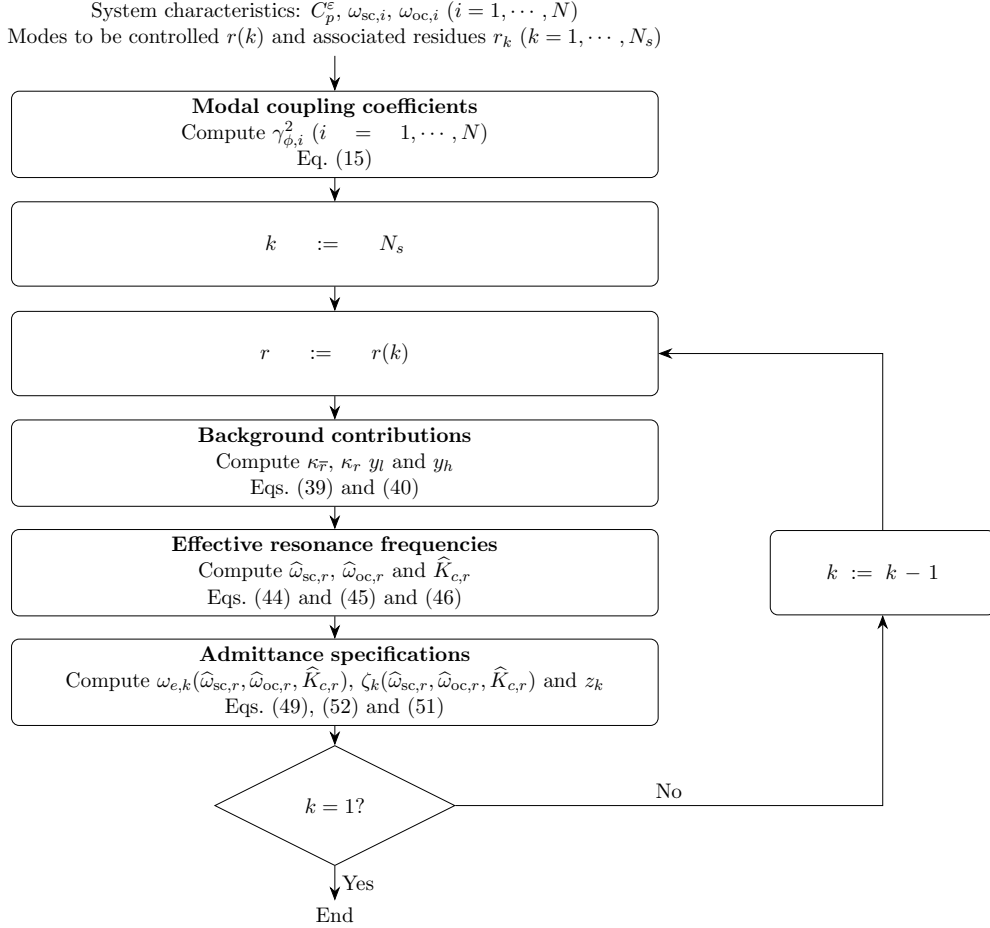


Figure 2: Flowchart of the proposed admittance-based specification approach.

Ideally, the shunt admittance  $Y_s$  should be chosen such that Norton's dissipative admittance is of the form

$$Y_N(s) = sC_p^\varepsilon + Y_s(s) = sC_p^\varepsilon \left( r_0 + \sum_{i=1}^{N_s} \frac{r_i s^2}{s^2 + 2\zeta_i z_i s + z_i^2} \right)^{-1}. \quad (53)$$

### 3.2. Impedance-based model

Similar developments to those of Section 3.1.1 can be made from Eq. (2). In this case, Thévenin's equivalent impedance of the series connection of the shunt with a capacitor of capacitance  $C_p^\varepsilon$ , given by

$$Z_T(s) = \frac{1}{sC_p^\varepsilon} + Z_s(s) \quad (54)$$

plays the same role here as Norton's admittance. A similar approach (not fully exposed here for brevity) can be followed to specify the characteristics of Thévenin's equivalent impedance.

Following the same approach as in Section 3.1.1 from Eqs. (9) and (54), it can be shown that the problem of a piezoelectric structure with a shunt can be cast as a feedback one where the controller is  $s^{-1}Z_T^{-1}(s)$ . In the special case where only an inductor of inductance  $L$  (i.e., a lossless RL shunt) is connected to the transducer, the transfer function of this equivalent controller takes the form

$$\frac{1}{sZ_T(s)} = \frac{1}{\frac{1}{C_p^\varepsilon} + Ls^2} = C_p^\varepsilon \frac{1}{\frac{s^2}{\omega_e^2} + 1}, \quad (55)$$

whose electrical resonance frequency is given by  $\omega_e^{-2} = LC_p^\varepsilon$ .

### 3.2.1. Implications of Foster's reactance theorem

Foster's reactance theorem [31, 32] can be used to deduce several properties of  $Z_T(s)$  with a lossless shunt, namely, to show that it takes the general form

$$\frac{1}{sZ_T(s)} = C_p^\varepsilon \left( r_0 + \sum_{i=1}^{N_s} \frac{r_i}{\frac{s^2}{z_i^2} + 1} \right), \quad (56)$$

where  $z_i$  is a zero of Thévenin's impedance, and  $r_i$  is its associated residue. Again, Eq. (56) can be seen as a generalization of Eq. (55) to multiple electrical resonances, the residues representing their amplitudes. Analyzing the properties of Eq. (56) for  $s \rightarrow 0$  shows that the residues must satisfy the passivity constraints

$$r_i \geq 0 \quad \forall i \in [0, N_s], \quad 0 \leq \sum_{i=0}^{N_s} r_i \leq 1. \quad (57)$$

### 3.2.2. Effective short-circuit and open-circuit resonance frequencies and coupling assessment

It is assumed that mode  $k$  of Thévenin's impedance targets resonance  $r$  of the structure, that the lower- and higher-frequency electrical modes are inductively- and capacitively-dominated, i.e.,

$$\frac{r_i}{\frac{s^2}{z_i^2} + 1} \approx \frac{r_i z_i^2}{s^2}, \quad i < k, \quad \text{and} \quad \frac{r_i}{\frac{s^2}{z_i^2} + 1} \approx r_i, \quad i > k, \quad (58)$$

respectively, and that the non-resonant mechanical modes contribute only through static response of the higher-frequency modes. The following quantities are introduced

$$\kappa_{\bar{r}} = \sum_{n=r+1}^N \frac{\theta_{\phi,n}^2 C_p^\varepsilon}{\omega_{oc,n}^2}, \quad \kappa_r = \sum_{n=r}^N \frac{\theta_{\phi,n}^2 C_p^\varepsilon}{\omega_{oc,n}^2}, \quad (59)$$

and

$$z_l = \sum_{i=1}^{k-1} \frac{r_i z_i^2}{\omega_{oc,r}^2}, \quad z_h = r_0 + \sum_{i=k+1}^{N_s} r_i. \quad (60)$$

Retaining a pair of mechanical and electrical resonant modes, and with the aforementioned approximations, the following equation is obtained

$$\left( \begin{array}{c} z_l \frac{\omega_{oc,r}^2}{s^2} + \frac{r_k}{s^2} + z_h \\ \frac{z_k^2}{z_k^2} + 1 \\ s^2 + \omega_{oc,r}^2 - \omega_{oc,r}^2(\kappa_r - \kappa_{\bar{r}}) \frac{z_l \frac{\omega_{oc,r}^2}{s^2} + \frac{r_k}{s^2} + z_h}{z_k^2} \\ 1 - \kappa_{\bar{r}} \left( z_l \frac{\omega_{oc,r}^2}{s^2} + \frac{r_k}{s^2} + z_h \right) \frac{z_k^2}{z_k^2} + 1 \end{array} \right) \eta_{oc,r} = 0. \quad (61)$$

Effective short- and open-circuit resonance frequencies can be found from Eq. (61) as

$$\widehat{\omega}_{sc,r} = \omega_{oc,r} \sqrt{\frac{1 - z_l \kappa_{\bar{r}} - (z_h + r_k) \kappa_r}{2 - 2(z_h + r_k) \kappa_{\bar{r}}} + \sqrt{\left( \frac{1 - z_l \kappa_{\bar{r}} - (z_h + r_k) \kappa_r}{2 - 2(z_h + r_k) \kappa_{\bar{r}}} \right)^2 + \frac{z_l \kappa_r}{1 - (z_h + r_k) \kappa_{\bar{r}}}}}, \quad (62)$$

and

$$\widehat{\omega}_{oc,r} = \omega_{oc,r} \sqrt{\frac{1 - z_l \kappa_{\bar{r}} - z_h \kappa_r}{2 - 2z_h \kappa_{\bar{r}}} + \sqrt{\left( \frac{1 - z_l \kappa_{\bar{r}} - z_h \kappa_r}{2 - 2z_h \kappa_{\bar{r}}} \right)^2 + \frac{z_l \kappa_r}{1 - z_h \kappa_{\bar{r}}}}}, \quad (63)$$

respectively. From the MEMCF given in Eq. (46), we note the following particular cases

$$\widehat{K}_{c,r}^2 \Big|_{r_k=0} = 0, \quad \widehat{K}_{c,r}^2 \Big|_{r_k=1} = K_{c,r}^2 \quad (64)$$

and it is possible to show that  $\widehat{\omega}_{sc,r}$  is a decreasing function of  $r_k$ , and thus  $\widehat{K}_{c,r}$  is a growing function of  $r_k$ .

A more explicit expression of  $\widehat{K}_{c,r}$  as a function of  $r_k$  can be obtained if one neglects the influence of non-resonant terms ( $z_l = z_h = \kappa_{\bar{r}} = 0$ ). The effective short- and open-circuit resonance frequencies are then estimated by

$$\widehat{\omega}_{sc,r}^2 \approx \omega_{oc,r}^2 (1 - r_k \theta_{\phi,r}^2 C_p^\epsilon), \quad \widehat{\omega}_{oc,r}^2 \approx \omega_{oc,r}^2. \quad (65)$$

The MEMCF is

$$\widehat{K}_{c,r}^2 \approx \frac{r_k K_{c,r}^2}{1 + K_{c,r}^2 - r_k K_{c,r}^2} \stackrel{K_{c,r}^2 \ll 1}{\approx} r_k K_{c,r}^2. \quad (66)$$

Again, it can be observed that the MEMCF can be predicted from the residue with a rather simple formula. This highlights the same performance trade-off as in the admittance-based models.

### 3.2.3. Specifications for the shunt

As in the admittance-based model case, it is possible to set an electrical resonance frequency and associated damping ratio based on the effective modal characteristics of the electromechanical system. The formulæ from the SDoF baseline case can be used to specify the electrical resonance

frequency  $\omega_{e,k}$  and damping ratio  $\zeta_{e,k}$ , as in Section 3.1.7. To obtain a zero of the mechanical receptance in Eq. (61),  $z_k$  should satisfy

$$z_k = \frac{\omega_{e,k}}{\sqrt{1 - \frac{r_k}{\frac{1}{\kappa_{\bar{r}}} + z_l \frac{\omega_{oc,r}^2}{\omega_{e,k}^2} - z_h}}}. \quad (67)$$

It is now possible to devise a specification procedure for the shunt's characteristics. From a set of modes to be controlled and associated residues, the zeros of Thévenin's impedance and the desired damping for optimal vibration reduction can be computed. Eq. (58) shows that in order to tune  $z_k$ ,  $z_1$  to  $z_{k-1}$  have to be known, which suggests that the tuning must be done in ascending order of frequency. Fig. 3 summarizes the proposed approach.

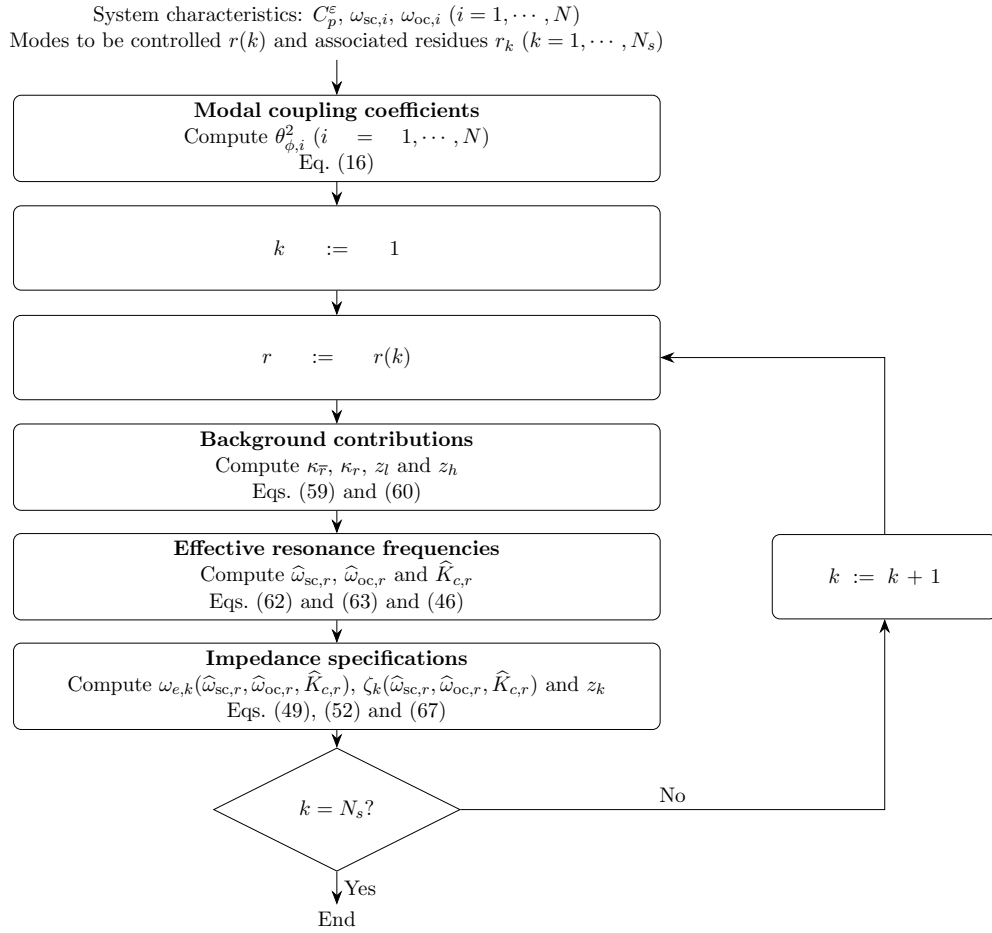


Figure 3: Flowchart of the proposed impedance-based specification approach.

With these specifications, the shunt impedance  $Z_s$  should ideally be such that Thévenin's

dissipative impedance is

$$Z_T(s) = \frac{1}{sC_p^\varepsilon} + Z_s(s) = \frac{1}{sC_p^\varepsilon} \left( r_0 + \sum_{i=1}^{N_s} \frac{r_i}{\frac{s^2}{z_i^2} + 2\zeta_i \frac{s}{z_i} + 1} \right)^{-1}. \quad (68)$$

### 3.3. Equivalence between the models

Two types of specification procedures were developed in the previous sections. They both yield a set of frequencies  $z_i$  and a set of associated damping ratios  $\zeta_i$ . Whether the admittance-based or impedance-based specification is used, these parameters will be very close provided they use the same baseline case, but not rigorously identical. The small discrepancies come from the difference in the frequencies around which the approximations are made (either short- or open-circuit resonance frequencies), and are generally negligible in front of the other approximations.

It is now shown that the two approaches are equivalent in the lossless case (assuming identical frequencies  $z_i$ ), but not in the dissipative case (assuming identical frequencies  $z_i$  and damping ratios  $\zeta_i$ ).

The shunt admittance is the inverse of the shunt impedance, i.e.,

$$Y_s(s) = \frac{1}{Z_s(s)}. \quad (69)$$

Thus, a relation between Norton's admittance defined in Eq. (24) and Thévenin's impedance defined in Eq. (54) can be derived as

$$Y_N(s) = \frac{sC_p^\varepsilon Z_T(s)}{Z_T(s) - \frac{1}{sC_p^\varepsilon}}, \quad Z_T(s) = \frac{Y_N(s)}{sC_p^\varepsilon(Y_N(s) - sC_p^\varepsilon)}. \quad (70)$$

#### 3.3.1. Lossless case

In the lossless case, if Norton's admittance is given by Eq. (24), then, by Eq. (70), one obtains

$$\frac{1}{sZ_T(s)} = C_p^\varepsilon \left( 1 - \sum_{i=0}^{N_s} r_i + \sum_{i=1}^{N_s} \frac{r_i}{\frac{s^2}{z_i^2} + 1} \right), \quad (71)$$

which is of the same form as Eq. (54) (the only difference being the expression of  $r_0$ ). Specifically, the zeros of  $Z_T$  are identical to those of  $Y_N$ , and their associated residues are also identical. Thus, the two approaches are equivalent in the lossless case. While passing from one model to the other, it should be kept in mind that all the residues stay identical except for  $r_0$ , which becomes

$$r_0 := 1 - \sum_{i=0}^{N_s} r_i. \quad (72)$$

### 3.3.2. Dissipative case

If dissipative circuits are considered, Norton's dissipative admittance would ideally be given by Eq. (53), while Thévenin's dissipative impedance would ideally be given by Eq. (68). Inserting Eq. (53) into Eq. (70), the following expression is obtained after transforming Norton's admittance to Thévenin's impedance:

$$\frac{1}{sZ_T(s)} = C_p^\varepsilon \left( 1 - r_0 - \sum_{i=1}^{N_s} \frac{r_i \left( 2\zeta_i \frac{s}{z_i} + 1 \right)}{\frac{s^2}{z_i^2} + 2\zeta_i \frac{s}{z_i} + 1} \right). \quad (73)$$

This shows that when dissipative circuits are considered ( $\zeta_i \neq 0$ ), the two approaches are no longer completely equivalent, because Eqs. (68) and (73) do not have the same form. The damping ratios are generally moderately small, so the discrepancy is moderate as well.

## 4. Shunt realization

### 4.1. Shunt admittance

If the shunt specifications come from an admittance-based approach (Section 3.1), the shunt admittance can then be determined from Eqs. (24) and (53),

$$Y_s(s) = Y_N(s) - sC_p^\varepsilon = sC_p^\varepsilon \frac{1 - r_0 - \sum_{i=1}^{N_s} \frac{r_i s^2}{s^2 + 2\zeta_i z_i s + z_i^2}}{r_0 + \sum_{i=1}^{N_s} \frac{r_i s^2}{s^2 + 2\zeta_i z_i s + z_i^2}}. \quad (74)$$

This model works best if the admittance is tuned with the parallel RL baseline. Conversely, if the shunt specifications come from an impedance-based approach (Section 3.2), the shunt admittance can then be determined from Eqs. (54) and (68) as

$$Y_s(s) = \frac{1}{Z_s(s)} = \frac{1}{Z_T(s) - \frac{1}{sC_p^\varepsilon}} = sC_p^\varepsilon \frac{r_0 + \sum_{i=1}^{N_s} \frac{r_i}{\frac{s^2}{z_i^2} + 2\zeta_i \frac{s}{z_i} + 1}}{1 - r_0 - \sum_{i=1}^{N_s} \frac{r_i}{\frac{s^2}{z_i^2} + 2\zeta_i \frac{s}{z_i} + 1}}. \quad (75)$$

This model works best if the admittance is tuned with the series RL baseline.

It is interesting to note that similar forms to Eqs. (74) and (75) were proposed by Moheimani et al [13, 15, 35] by casting the passive control problem into a feedback one and using Youla's parametrization of all stabilizing controllers. However, the role of the residues was not as thoroughly discussed as here, and the tuning procedure was different for  $z_i$  (set equal to the corresponding open-circuit resonance frequency therein) and  $\zeta_i$  (tuned by an optimization algorithm therein), which are tuned based on the SDoF formulae herein (see Appendix A).

#### 4.2. Digital vibration absorber

Eqs. (74) and (75) specify the shunt admittance by its transfer function but neither specify the circuit topology, nor the associated electrical parameters. Similarly to [18], a synthesis method such as Brune’s [36] could be used to realize the passive shunt. Alternatively, a DVA such as depicted in Fig. 4 can enable the realization of virtually any shunt through programming of its admittance as the transfer function of the digital unit [23].

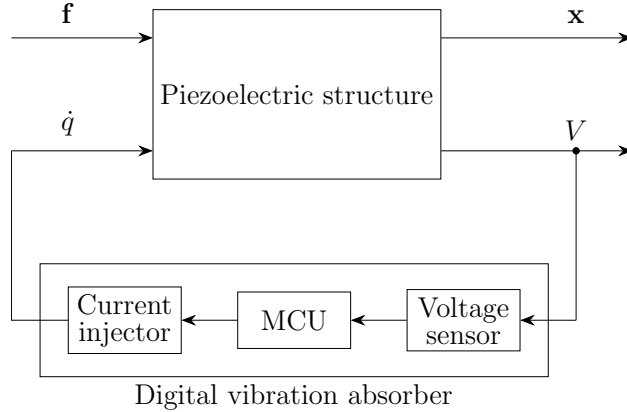


Figure 4: General working principle of the DVA.

The passivity of the emulated circuit guarantees the unconditional stability of the control law. However, the finite phase margin associated to this type of control may call for a method allowing to prevent delay-induced instabilities [37].

### 5. Numerical verification

The cantilever beam that first appeared in Thomas et al [25] and was later studied in several works [20, 28, 30, 38] is used as a first example to numerically demonstrate the proposed approach. It is a clamped-free aluminum beam on which two PIC 151 piezoelectric patches are symmetrically bonded, as depicted in Fig. 5. The geometrical and material properties of the system were taken from [25] and are reported in Tables 1 and 2. The patches have opposite polarization, and they are connected in series to form one equivalent piezoelectric transducer. A finite element model was built with Euler-Bernoulli beam elements following the procedure described in [25]. The beam was discretized with 1, 5 and 35 elements for  $x \in [0, x_-]$ ,  $x \in [x_-, x_+]$  and  $x \in [x_+, l]$ , respectively. Accounting for the clamped boundary condition, this resulted in a model with 123 mechanical DoFs. The series connection of the patches adds one electrical DoF to the model.

$l$	$b$	$t$	$\rho$	$E$
170 mm	20 mm	2 mm	2800 kg m <sup>-3</sup>	72 GPa

Table 1: Parameters of the cantilever piezoelectric beam from [25].

The beam is transversely excited on its free end. Modal damping was set to 0.1% on all the modes. The driving-point frequency response function (FRF) therefore exhibits lightly-damped resonances which can be targeted by the above-mentioned shunts in order to reduce the vibratory

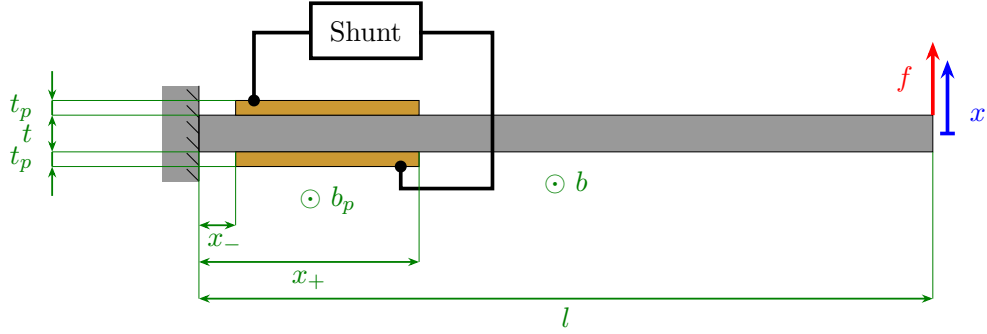


Figure 5: Schematic representation of the cantilever piezoelectric beam from [25].

$l_p$	$b_p$	$t_p$	$x_-$	$x_+$	$\rho_p$	$E_p$	$d_{31}$	$\epsilon_{33}^\epsilon$
25 mm	20 mm	0.5 mm	0.5 mm	25.5 mm	$8500 \text{ kg m}^{-3}$	66.7 GPa	-210	$2068\epsilon_0$

Table 2: Parameters of the piezoelectric patches from [25], where  $\epsilon_0=8.854 \text{ pF m}^{-1}$ .

amplitude. The three first bending modes frequencies of the beam with short-circuited patches are 68.89 Hz, 411.28 Hz and 1092.86 Hz, in accordance with [38] (but slightly differ from [25] because a tip mass was added therein to agree with experimental results).

### 5.1. Control of two structural modes

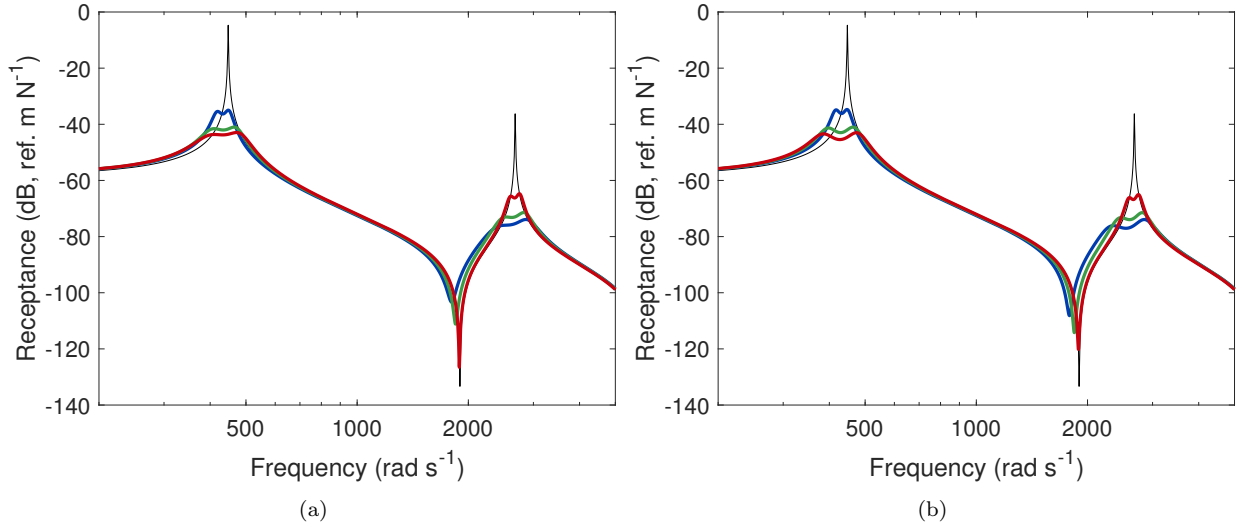


Figure 6: FRF of the beam with open-circuited patches (—) and controlled with a circuit with ideal Thévenin's impedance (a) and ideal Norton's admittance (b):  $r_1 = 0.1$ ,  $r_2 = 0.9$  (—),  $r_1 = 0.5$ ,  $r_2 = 0.5$  (—) and  $r_1 = 0.9$ ,  $r_2 = 0.1$  (—).

The first two bending modes of the beam are targeted at first to keep the exposition simple. Fig. 6 presents the FRFs of the controlled beam with both approaches (yielding ideal Norton's admittance and Thévenin's impedance), using various values of the residues associated with modes 1 ( $r_1$ ) and 2 ( $r_2$ ), while respecting the passivity constraint  $r_1 + r_2 = 1$ . Both techniques yield similar performance in terms of vibration reduction, given identical residues. As expected, the greater  $r_1$

the greater the vibration attenuation on mode 1, but the smaller the vibration attenuation on mode 2. The residues can thus be set to balance the control authority on specific modes, at the expense of that on other modes.

The impact of the residues on the vibration reduction of the modes is also confirmed in Fig. 7, where the attenuation on each mode (defined as the ratio of the uncontrolled FRF at  $\omega_{sc,r}$  to the controlled FRF at the effective open-circuit resonance frequency  $\hat{\omega}_{oc,r}$ ) is plotted against the value of the residue<sup>2</sup>  $r_1$  (and  $r_2 = 1 - r_1$ ). This attenuation is compared to the prediction formula in [28] (Equation (35) therein), using the MEMCF predicted from the residues (Eq. (48) or (66)). The prediction formula agrees well with the measured attenuation when the associated residue is high. It underestimates the attenuation when the residue is low because it overlooks the action of the non-resonant electrical modes on resonant mechanical modes. For instance, it can be seen in Fig. 7(a) that a series RL shunt on mode 2 (the limit case when  $r_2 = 1$ ) can have a non-negligible attenuation effect on mode 1 and the converse is also true for a parallel RL shunt. Although not directly aimed at resonant shunts, this aspect is discussed more in depth in [39]. In any case, the observed trends verify the relevance of using an MEMCF such as defined in Eq. (46), and its predicted approximation Eq. (48) (or Eq. (66)) to guide the choice of the residues.

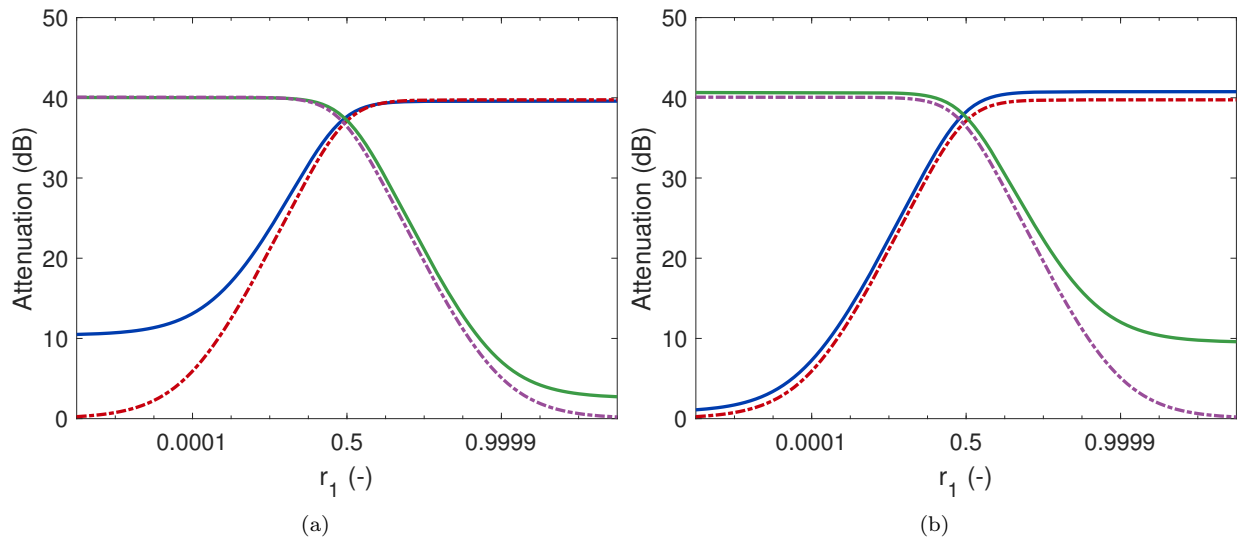


Figure 7: Attenuation of the modes as a function of the first residue for a circuit with ideal Thévenin's impedance (a) and ideal Norton's admittance (b): attenuation computed from the FRF (— : mode 1, — : mode 2) and attenuation predicted with [28] using a linearized MEMCF (--- : mode 1, --- : mode 2).

## 5.2. Control of five structural modes

The proposed method can handle an arbitrary number of modes. To illustrate this, Fig. 8 compares the FRF of the beam with open-circuit patches to those with ideal shunts using identical residues on each targeted mode ( $r_i = 0.2$ ,  $i = 1, \dots, 5$ ). The five resonances are effectively mitigated with both approaches. For comparison purposes, the tuning method from [15] was also applied to that case. While similar performance is observed with the ideal Norton's admittance, the

<sup>2</sup>The unusual scale for the abscissa in these figures is given by  $\log_{10}(r_1/(1-r_1))$  in order to enlarge the regions where  $r_1 \approx 0$  and  $r_1 \approx 1$ .

control authority over the last four modes is degraded with the ideal Thévenin's impedance. This comes from the optimization algorithm, which tries to minimize the  $H_2$  norm of the receptance by focusing on the first mode, thereby neglecting the other modes. Hence, the outcome of the proposed method is at worst comparable with the method from [15], and is much faster since it does not rely on numerical optimization (there was a speedup factor of 200 in the computation of the parameters of the shunt admittances between the method proposed herein and that proposed therein).

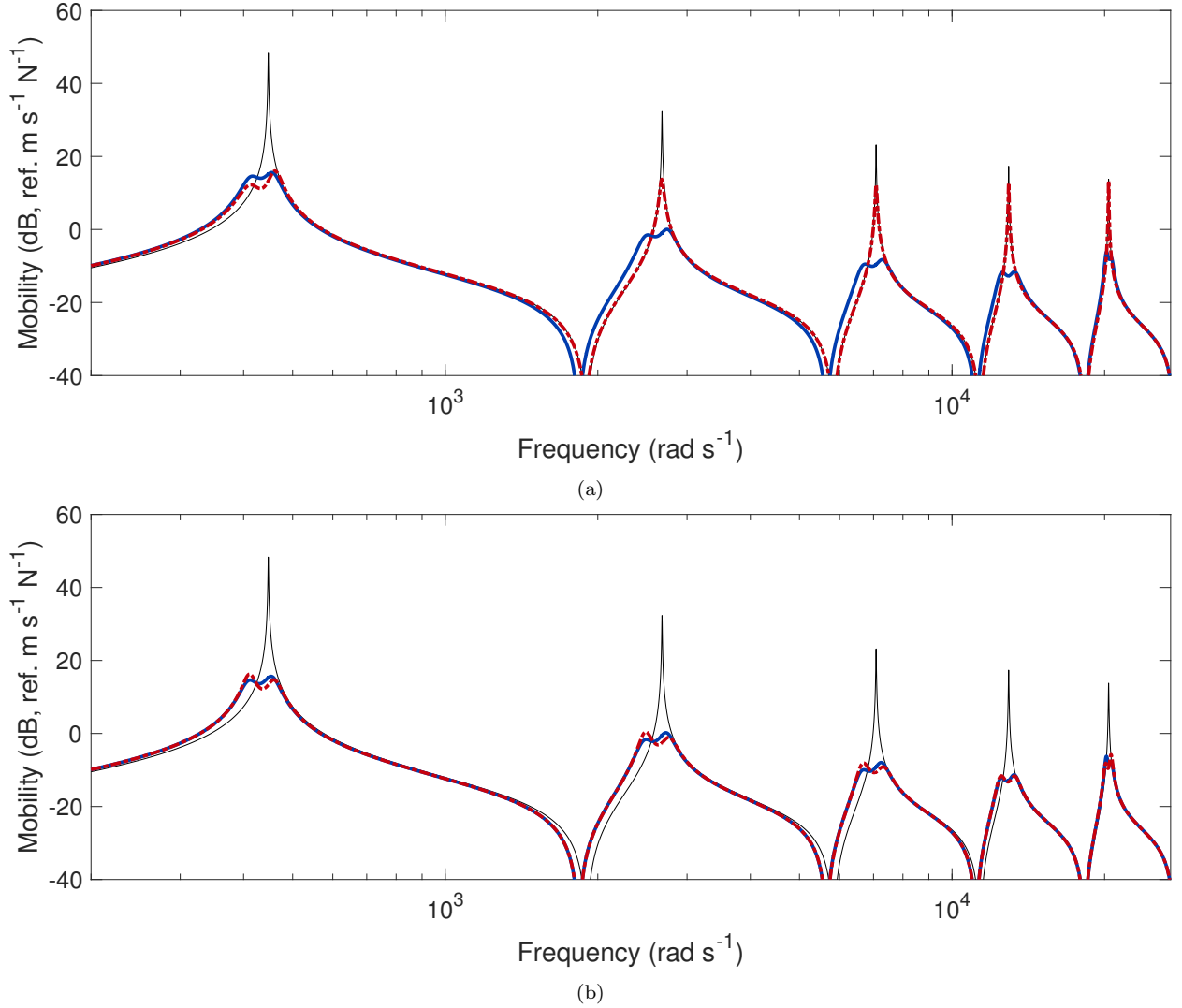


Figure 8: Mobility of the beam with open-circuited patches (—) and controlled with a circuit with ideal Thévenin's impedance (a) and ideal Norton's admittance (b) (—: proposed method, - - -: method from [15]).

## 6. Experimental validation

The clamped-free piezoelectric beam shown in Fig. 9 and schematically represented in Fig. 10 was used as a host to experimentally validate the theoretical developments. The free end of the

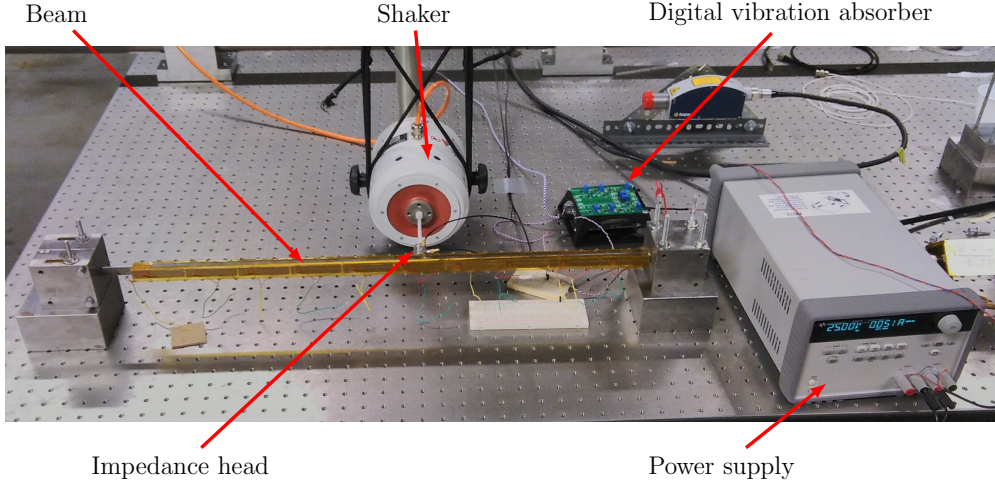


Figure 9: Picture of the experimental setup.

beam is attached to a thin lamina. This thin lamina can be responsible for a hardening behavior of the beam (see, e.g., [40]), but the forcing levels in this experimental study were kept low enough to make this nonlinear effect negligible. Details about the geometrical dimensions of the beam and the patches are given in Tables 3 and 4, respectively. The beam was excited at mid-span by an electrodynamic shaker, and an impedance head was used to measure the acceleration and force of the structure. The two first bending modes of the beam were targeted for shunt damping. The steel beam is covered by an array of ten pairs of uniformly distributed PSI-5A4E piezoelectric patches (each pair consisting of two patches connected in parallel). Two of these pairs were connected in parallel to form one equivalent piezoelectric transducer in order to balance the MEMCFs of these modes. The other eight pairs were left in open circuit.

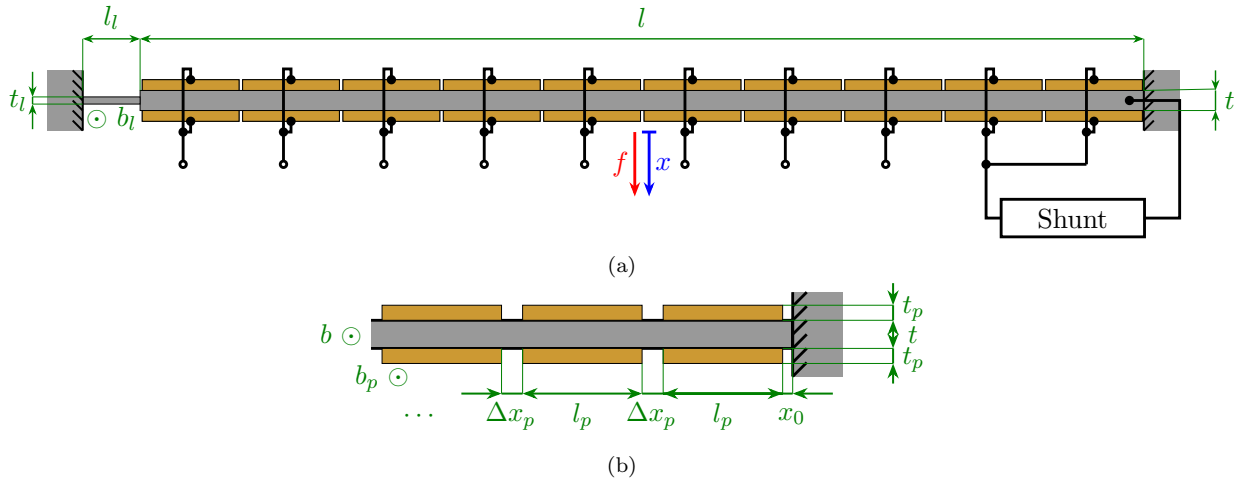


Figure 10: Schematic representation of the clamped-free piezoelectric beam with a thin lamina: overall view (a) and close-up on the patches close to the clamped end (b).

The approach to implement a multimodal shunt experimentally is fairly straightforward thanks to its model-less nature. The peaks of the FRFs of the structure with short- and open-circuited

$l$	$b$	$t$	$l_l$	$b_l$	$t_l$
700 mm	14 mm	14 mm	40 mm	14 mm	0.5 mm

Table 3: Parameters of the clamped-free piezoelectric beam with a thin lamina.

$l_p$	$b_p$	$t_p$	$x_0$	$\Delta x_p$
67 mm	14 mm	2 mm	1 mm	3 mm

Table 4: Parameters of the piezoelectric patches of the clamped-free piezoelectric beam with a thin lamina.

patches were used to estimate the short- and open-circuit resonance frequencies, and the capacitance of the patches was measured with a multimeter. All these parameters are reported in Table 5. From there on, the approaches outlined in Figs. 2 and 3 were followed, and the obtained admittances were emulated by a DVA. Delay-induced instabilities were also suppressed using the method described in [37].

$f_{sc,1}$	$f_{oc,1}$	$K_{c,1}$	$f_{sc,2}$	$f_{oc,2}$	$K_{c,2}$	$C_p^\epsilon$
31.36 Hz	31.49 Hz	0.091	144.55 Hz	144.92 Hz	0.072	99 nF

Table 5: Parameters of the experimental setup.

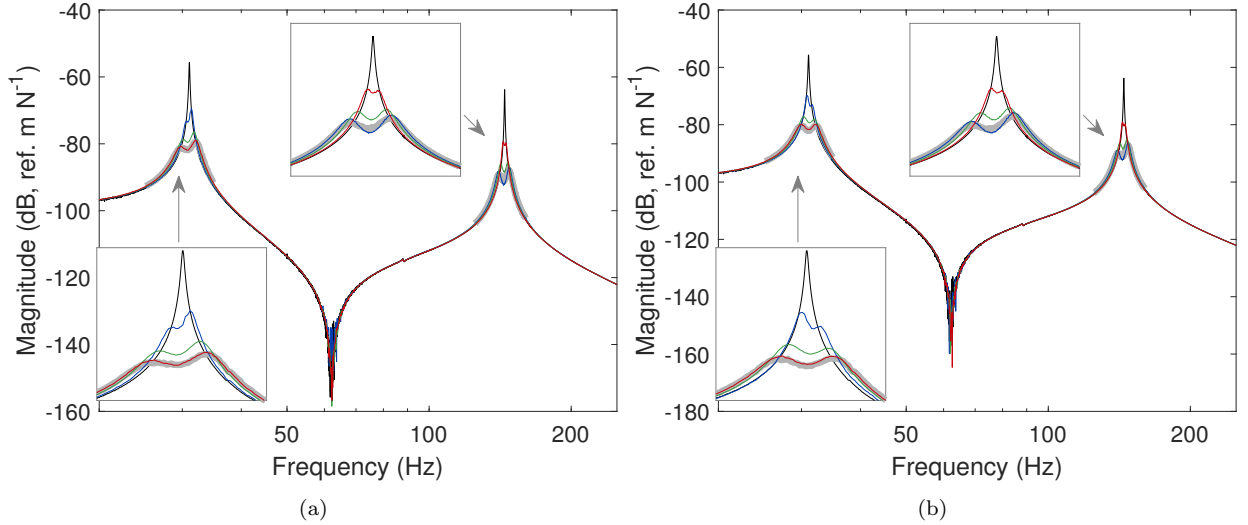


Figure 11: Experimental FRF of the beam with open-circuited patches (—) and controlled with a shunt with ideal Thévenin's impedance (a) and ideal Norton's admittance (b):  $r_1 = 0.1$ ,  $r_2 = 0.9$  (—),  $r_1 = 0.5$ ,  $r_2 = 0.5$  (—) and  $r_1 = 0.9$ ,  $r_2 = 0.1$  (—). Thick gray lines indicate the FRF of the beam controlled with single-mode series (a) or parallel (b) RL shunts.

The ideal impedance and admittance described in Section 4.1 were used to obtain the FRFs featured in Fig. 11, obtained for various values of the residues  $r_1$  and  $r_2 = 1 - r_1$ . These experimental results validate the analysis presented in this paper: the DVA is able to control the two modes, and the control authority over the modes can be traded off with the residues. Moreover, the performance of the two shunt types is similar, and tends to a single-mode shunt of associated type on a specific mode when the residue associated to that mode tends to one.

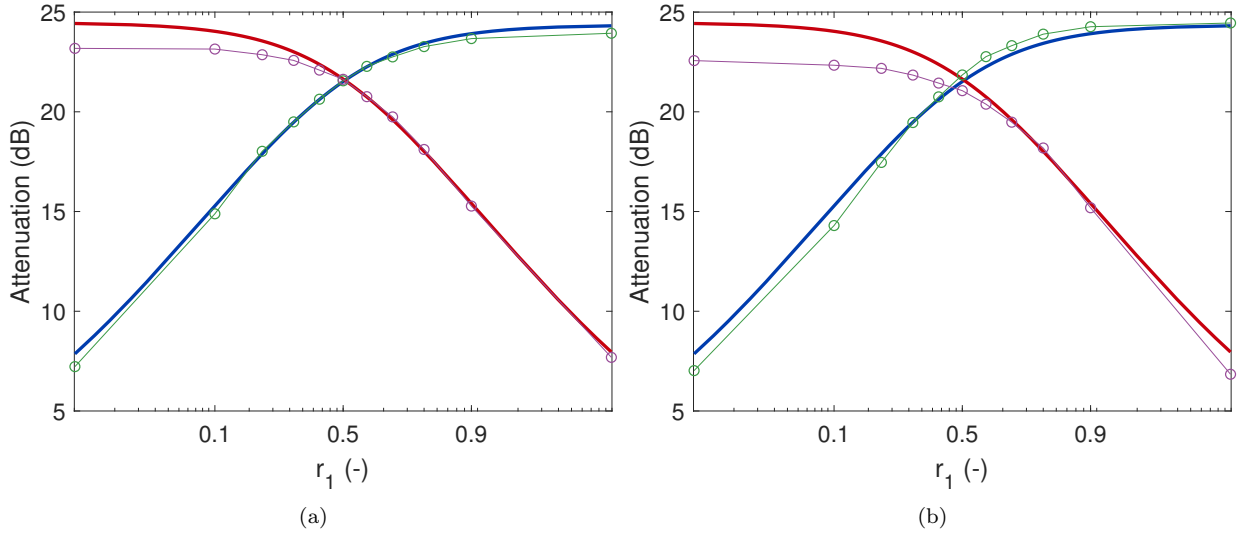


Figure 12: Experimental attenuation of the two first modes of the beam with a shunt with ideal Thévenin's impedance (a) and ideal Norton's admittance (b): mode 1 (— : prediction [28], -o-: measurement) and mode 2 (— : prediction [28], -o-: measurement).

A more thorough analysis was pursued by measuring the FRFs for more values of the residues. All these FRFs are not shown for brevity but Fig. 12 summarizes their information, by providing the attenuation as a function of  $r_1$ . The experimental results were compared to the theoretical formula from [28]. To use this formula, the damping ratio on both modes was estimated from the short-circuit FRF using the half-power method. Again, an excellent agreement with theory is obtained, except for small  $r_1$ . The attenuation in mode 2 is somewhat overestimated by the prediction, which could be explained by the slightly underdamped appearance of the peaks associated with mode 2 in Fig. 11.

## 7. Conclusion

The generalization of classical RL shunts to circuits having multiple electrical resonances allows for the control of multiple structural modes. After reviewing the dynamics of multiple-degree-of-freedom piezoelectric structures, a sequential specification procedure was proposed to tune the characteristics of a shunt. The cornerstone of this method consists in approximating the dynamics of the controlled system by an effective one around a pair of mechanical and electrical resonances, and leveraging the single-mode formulae. The shunt admittance can then be determined and emulated by a DVA. The theoretical developments were numerically verified and experimentally validated on piezoelectric beams.

The proposed approach provides effective mitigation of multiple resonances while being easy to implement and usable with readily-obtainable experimental measurements. The free parameters chosen by the designer, i.e., the residues, can also clearly be linked to the performance of the resulting shunt.

Future works may involve the synthesis and realization of optimal shunts made out of passive electrical components, as well as the generalization of this work to control with multiple piezoelectric transducers.

## Acknowledgements

Funding: This work was supported by the SPW [WALInnov grant 1610122].

## Appendix A. Tuning formulae for single-mode RL shunts

### Appendix A.1. Series RL shunt

The optimal tuning of a series RL shunt has been found in [4, 5]. Introducing an intermediate parameter

$$r = \frac{\sqrt{64 - 16K_c^2 - 26K_c^4} - K_c^2}{8}, \quad (\text{A.1})$$

the optimal frequency ratio is

$$\delta(K_c) = \sqrt{\frac{3K_c^2 - 4r + 8}{4K_c^2 + 4}} \quad (\text{A.2})$$

and the optimal damping ratio is

$$\zeta(K_c) = \frac{\sqrt{27K_c^4 + 80K_c^2 + 64 - 16r(4 + 3K_c^2)}}{\sqrt{2}(5K_c^2 + 8)}. \quad (\text{A.3})$$

### Appendix A.2. Parallel RL shunt

The optimal tuning of a parallel RL shunt has been found in [5]. The following parameters are introduced:

$$\begin{aligned} b_0 &= 64 & b_1 &= -16K_c^2 \\ b_2 &= -64 + 16K_c^2 + 11K_c^4 & b_3 &= 2K_c^2(8 - K_c^2)(2 - K_c^2) \\ b_4 &= -2K_c^4(2 - K_c^2) & a_5 &= 12b_0b_4 - 3b_1b_3 + b_2^2 \\ a_6 &= 27(b_0b_3^2 + b_1^2b_4) - 9b_2(b_1b_3 + 8b_0b_4) + 2b_2^3 & a_3 &= \frac{1}{2} \sqrt{\frac{b_1^2}{b_0^2} + \frac{4(a_4^2 + a_5 - 2b_2a_4)}{3b_0a_4}} \\ a_4 &= \sqrt[3]{\frac{\sqrt{a_6^2 - 4a_5^3} + a_6}{2}} & a_1 &= \frac{3b_1^2a_4 - 2b_0(4b_2a_4 + a_4^2 + a_5)}{6b_0^2a_4} \\ a_2 &= -\frac{8b_0^2b_3 - 4b_0b_1b_2 + b_1^3}{4b_0^3a_3} \end{aligned} \quad (\text{A.4})$$

Eventually,

$$r = -\frac{b_1}{4b_0} + \frac{a_3}{2} + \frac{\sqrt{a_1 + a_2}}{2}, \quad (\text{A.5})$$

the optimal reluctance frequency ratio is

$$\nu(K_c) = \sqrt{\frac{2r - K_c^2 + \sqrt{16r^2 - 4rK_c^2 + K_c^4}}{6}} \quad (\text{A.6})$$

and the optimal damping ratio is

$$\varsigma(K_c) = \sqrt{\frac{(r-1)(3r-2K_c^2)}{r(2r+K_c^2-\sqrt{16r^2-4rK_c^2+K_c^4})}}. \quad (\text{A.7})$$

## References

- [1] R. L. Forward, Electronic damping of vibrations in optical structures, *Appl. Opt.* 18 (5) (1979) 690. doi:10.1364/AO.18.000690.  
URL <https://www.osapublishing.org/abstract.cfm?URI=ao-18-5-690>
- [2] N. Hagood, A. von Flotow, Damping of structural vibrations with piezoelectric materials and passive electrical networks, *J. Sound Vib.* 146 (2) (1991) 243–268. doi:10.1016/0022-460X(91)90762-9.  
URL <https://linkinghub.elsevier.com/retrieve/pii/0022460X91907629>
- [3] S.-y. Wu, Piezoelectric shunts with a parallel R-L circuit for structural damping and vibration control, in: C. D. Johnson (Ed.), *Spie*, Vol. 2720, 1996, pp. 259–269. doi:10.1117/12.239093.  
URL <http://proceedings.spiedigitallibrary.org/proceeding.aspx?articleid=1017503>
- [4] P. Soltani, G. Kerschen, G. Tondreau, A. Deraemaeker, Piezoelectric vibration damping using resonant shunt circuits: an exact solution, *Smart Mater. Struct.* 23 (12) (2014) 125014. doi:10.1088/0964-1726/23/12/125014.  
URL <http://stacks.iop.org/0964-1726/23/i=12/a=125014?key=crossref.798743ce34b627bed945b046d8a6b51a>
- [5] T. Ikegame, K. Takagi, T. Inoue, Exact Solutions to  $H_\infty$  and  $H_2$  Optimizations of Passive Resonant Shunt Circuit for Electromagnetic or Piezoelectric Shunt Damper, *J. Vib. Acoust. Trans. ASME* 141 (3) (2019). doi:10.1115/1.4042819.
- [6] G. A. Lesieutre, Vibration damping and control using shunted piezoelectric materials, *Shock and Vibration Digest* 30 (3) (1998) 187–195. doi:10.1177/058310249803000301.
- [7] M. Ahmadian, A. P. Degiulio, Recent advances in the use of piezoceramics for vibration suppression, *The Shock and Vibration Digest* 33 (1) (2001) 15–22. doi:10.1177/058310240103300102.
- [8] J. Gripp, D. Rade, Vibration and noise control using shunted piezoelectric transducers: A review, *Mechanical Systems and Signal Processing* 112 (2018) 359–383. doi:10.1016/j.ymssp.2018.04.041.  
URL <https://linkinghub.elsevier.com/retrieve/pii/S0888327018302437>
- [9] J. J. Hollkamp, Multimodal Passive Vibration Suppression with Piezoelectric Materials and Resonant Shunts, *J. Intell. Mater. Syst. Struct.* 5 (1) (1994) 49–57. doi:10.1177/1045389X9400500106.  
URL <http://journals.sagepub.com/doi/10.1177/1045389X9400500106>
- [10] S.-y. Wu, Method for multiple-mode shunt damping of structural vibration using a single PZT transducer, Vol. 3327, 1998, pp. 159–168. doi:10.1117/12.310680.  
URL <http://proceedings.spiedigitallibrary.org/proceeding.aspx?articleid=940157>
- [11] S. Behrens, S. O. R. Moheimani, A. J. Fleming, Multiple mode current flowing passive piezoelectric shunt controller, *J. Sound Vib.* 266 (5) (2003) 929–942. doi:10.1016/S0022-460X(02)01380-9.  
URL <https://linkinghub.elsevier.com/retrieve/pii/S0022460X02013809>
- [12] A. J. Fleming, S. Behrens, S. O. R. Moheimani, Reducing the inductance requirements of piezoelectric shunt damping systems, *Smart Mater. Struct.* 12 (1) (2003) 57–64. doi:10.1088/0964-1726/12/1/307.  
URL <http://stacks.iop.org/0964-1726/12/i=1/a=307?key=crossref.39ab51d3ef8ca1b6552bf22dd04b4ff3>
- [13] S. O. R. Moheimani, A. J. Fleming, *Piezoelectric Transducers for Vibration Control and Damping*, *Advances in Industrial Control*, Springer-Verlag, London, 2006. doi:10.1007/1-84628-332-9.  
URL <http://link.springer.com/10.1007/1-84628-332-9>
- [14] A. Fleming, S. Behrens, S. Reza Moheimani, Optimization and implementation of multimode piezoelectric shunt damping systems, *IEEE/ASME Trans. Mechatronics* 7 (1) (2002) 87–94. doi:10.1109/3516.990891.  
URL <http://ieeexplore.ieee.org/document/990891/>
- [15] S. Moheimani, A survey of recent innovations in vibration damping and control using shunted piezoelectric transducers, *IEEE Trans. Control Syst. Technol.* 11 (4) (2003) 482–494. doi:10.1109/TCST.2003.813371.  
URL <http://ieeexplore.ieee.org/document/1208326/>
- [16] J. Y. Jeon, Passive vibration damping enhancement of piezoelectric shunt damping system using optimization approach, *J. Mech. Sci. Technol.* 23 (5) (2009) 1435–1445. doi:10.1007/s12206-009-0402-8.
- [17] A. Cigada, S. Manzoni, M. Redaelli, M. Vanali, Optimization of the current flowing technique aimed at semi-passive multi-modal vibration reduction, *J. Vib. Control* 18 (2) (2012) 298–312. doi:10.1177/1077546311407537.  
URL <http://journals.sagepub.com/doi/10.1177/1077546311407537>
- [18] M. Berardengo, S. Manzoni, A. M. Conti, Multi-mode passive piezoelectric shunt damping by means of matrix inequalities, *J. Sound Vib.* 405 (2017) 287–305. doi:10.1016/j.jsv.2017.06.002.  
URL <http://dx.doi.org/10.1016/j.jsv.2017.06.002>
- [19] P. Gardonio, M. Zientek, L. D. Bo, Panel with self-tuning shunted piezoelectric patches for broadband flexural vibration control, *Mech. Syst. Signal Process.* 134 (2019) 1–32. doi:10.1016/j.ymssp.2019.106299.  
URL <https://doi.org/10.1016/j.ymssp.2019.106299>

- [20] G. Raze, A. Paknejad, G. Zhao, C. Collette, G. Kerschen, Multimodal vibration damping using a simplified current blocking shunt circuit, *J. Intell. Mater. Syst. Struct.* 31 (14) (2020) 1731–1747. doi:10.1177/1045389X20930103.  
URL <http://journals.sagepub.com/doi/10.1177/1045389X20930103>
- [21] B. Lossouarn, M. Aucejo, J.-F. Deü, B. Multon, Design of inductors with high inductance values for resonant piezoelectric damping, *Sensors Actuators A Phys.* 259 (2017) 68–76. doi:10.1016/j.sna.2017.03.030.  
URL <https://linkinghub.elsevier.com/retrieve/pii/S0924424716309785>
- [22] K. Dekemele, P. Van Torre, M. Loccufier, High-voltage synthetic inductor for vibration damping in resonant piezoelectric shunt, *J. Vib. Control* (2020) 107754632095261doi:10.1177/1077546320952612.  
URL <http://journals.sagepub.com/doi/10.1177/1077546320952612>
- [23] A. J. Fleming, S. Behrens, S. O. R. Moheimani, Synthetic impedance for implementation of piezoelectric shunt-damping circuits, *Electron. Lett.* 36 (18) (2000) 1525. doi:10.1049/el:20001083.  
URL <https://digital-library.theiet.org/content/journals/10.1049/el{ }20001083>
- [24] N. W. Hagood, W. H. Chung, A. Von Flotow, Modelling of Piezoelectric Actuator Dynamics for Active Structural Control, *Journal of Intelligent Material Systems and Structures* 1 (3) (1990) 327–354. doi:10.1177/1045389X9000100305.  
URL <http://journals.sagepub.com/doi/10.1177/1045389X9000100305>
- [25] O. Thomas, J.-F. Deü, J. Ducarne, Vibrations of an elastic structure with shunted piezoelectric patches: efficient finite element formulation and electromechanical coupling coefficients, *Int. J. Numer. Methods Eng.* 80 (2) (2009) 235–268. doi:10.1002/nme.2632.  
URL <http://doi.wiley.com/10.1002/nme.2632>
- [26] A. Preumont, *Vibration Control of Active Structures*, 3rd Edition, Vol. 179 of *Solid Mechanics and Its Applications*, Springer Netherlands, Dordrecht, 2011. doi:10.1007/978-94-007-2033-6.  
URL <http://link.springer.com/10.1007/978-94-007-2033-6>
- [27] G. F. Franklin, J. D. Powell, A. Emami-Naeini, *Feedback Control of Dynamic Systems*, Pearson London, 2015.
- [28] O. Thomas, J. Ducarne, J.-F. Deü, Performance of piezoelectric shunts for vibration reduction, *Smart Mater. Struct.* 21 (1) (2012) 015008. doi:10.1088/0964-1726/21/1/015008.  
URL <http://stacks.iop.org/0964-1726/21/i=1/a=015008?key=crossref.6d8696aab65a8889d18c15289623f766>
- [29] J. Høgsberg, S. Krenk, Calibration of piezoelectric RL shunts with explicit residual mode correction, *J. Sound Vib.* 386 (2017) 65–81. doi:10.1016/j.jsv.2016.08.028.  
URL <http://dx.doi.org/10.1016/j.jsv.2016.08.028>
- [30] J. F. Toftekær, A. Benjeddou, J. Høgsberg, Optimal piezoelectric resistive – inductive shunt damping of plates with residual mode correction, *J. Intell. Mater. Syst. Struct.* 29 (16) (2018) 3346–3370. doi:10.1177/1045389X18798953.
- [31] R. M. Foster, A Reactance Theorem, *Bell Syst. Tech. J.* 3 (2) (1924) 259–267. doi:10.1002/j.1538-7305.1924.tb01358.x.  
URL <http://ieeexplore.ieee.org/lpdocs/epic03/wrapper.htm?arnumber=6773392>
- [32] W.-K. Chen, *Passive, Active, and Digital Filters*, CRC Press, 2018. doi:10.1201/9781315219141.  
URL <https://www.taylorfrancis.com/books/9781420058864>
- [33] K. Yamada, H. Matsuhisa, H. Utsuno, K. Sawada, Optimum tuning of series and parallel LR circuits for passive vibration suppression using piezoelectric elements, *J. Sound Vib.* 329 (24) (2010) 5036–5057. doi:10.1016/j.jsv.2010.06.021.  
URL <http://dx.doi.org/10.1016/j.jsv.2010.06.021https://linkinghub.elsevier.com/retrieve/pii/S0022460X10004116>
- [34] J. Høgsberg, S. Krenk, Balanced calibration of resonant shunt circuits for piezoelectric vibration control, *J. Intell. Mater. Syst. Struct.* 23 (17) (2012) 1937–1948. doi:10.1177/1045389X12455727.  
URL <http://journals.sagepub.com/doi/10.1177/1045389X12455727>
- [35] S. Moheimani, S. Behrens, Multimode Piezoelectric Shunt Damping With a Highly Resonant Impedance, *IEEE Trans. Control Syst. Technol.* 12 (3) (2004) 484–491. doi:10.1109/TCST.2004.824318.  
URL <http://ieeexplore.ieee.org/document/1291419/>
- [36] O. Brune, Synthesis of a finite two-terminal network whose driving-point impedance is a prescribed function of frequency, Ph.D. thesis, Massachusetts Institute of Technology (1931).  
URL <https://dspace.mit.edu/bitstream/handle/1721.1/10661/36311006-MIT.pdf?sequence=2>
- [37] G. Raze, J. Dietrich, G. Kerschen, Onset and stabilization of delay-induced instabilities in piezoelectric digital vibration absorbers (2021). arXiv:2106.06715.
- [38] J. Ducarne, O. Thomas, J. F. Deü, Placement and dimension optimization of shunted piezoelectric patches for

- vibration reduction, *J. Sound Vib.* 331 (14) (2012) 3286–3303. doi:10.1016/j.jsv.2012.03.002.
- [39] M. Berardengo, S. Manzoni, M. Vanali, R. Bonsignori, Enhancement of the broadband vibration attenuation of a resistive piezoelectric shunt, *J. Intell. Mater. Syst. Struct.* (2021) 1045389X20988090doi:10.1177/1045389X20988090.  
URL <https://doi.org/10.1177/1045389X20988090>
- [40] B. Lossouarn, J. F. Deü, G. Kerschen, A fully passive nonlinear piezoelectric vibration absorber, *Philosophical Transactions of the Royal Society A: Mathematical, Physical and Engineering Sciences* 376 (2127) (2018). doi:10.1098/rsta.2017.0142.